Modulating the field-effect passivation at the SiO$_2$/c-Si interface: Analysis and verification of the photoluminescence imaging under applied bias method

Halvard Haug[1,*], Sara Olibet[2], Ørnulf Nordseth[1] and Erik Stensrud Marstein[1,3]

[1] Institute for Energy Technology, Instituttveien 18, 2007 Kjeller, Norway, s

[2] International Solar Energy Research Center-ISC Konstanz, Konstanz, Germany

[3] Department of Physics, University of Oslo, Pb 1048 Blindern 0316 Oslo, Norway

[*]Corresponding author: E-mail: halvard.haug@ife.no Phone: +47 99486756

_____

In this paper we study the surface passivation properties of thermally oxidized silicon wafers with controlled surface band bending, using a new characterization technique combining calibrated photoluminescence imaging with the application of an external voltage over the rear side passivation layer. Various aspects of the technique and possible errors in the determination of the effective surface recombination velocity are discussed, including lateral carrier diffusion, leakage currents and optical effects related to the presence of metal electrodes on the investigated samples. In order to quantitatively describe the recombination activity at the SiO$_2$/c-Si interface and the effect of fixed charges in the oxide layer the measured effective carrier lifetime vs. voltage curves have been analyzed in the framework of an extended Shockley-Read Hall recombination model. Furthermore, the results have been compared with corresponding results from microwave detected photoconductance decay measurements after depositing corona charges. We find an excellent agreement between the two techniques and between complementary measurements of the oxide charge density. Photoluminescence imaging under applied bias gives fast and repeatable measurements and allows for simultaneous data collection from multiple areas on the sample, and has thus been proven to be powerful tool for quantitative characterization of surface passivation layers.

I.   INTRODUCTION

Currently there is a large research activity focusing on the implementation of effective rear side surface passivation in the production of high efficiency Si solar cells. Most of these approaches use thin dielectric layers or stacks deposited by various thin film deposition methods like plasma enhanced chemical vapor deposition (PECVD) or atomic layer deposition (ALD). High-quality surface passivation may also be achieved by thermal oxidation, and thin

SiO_2 films have been demonstrated in industrial pilot production[1]. The passivating properties of these Si solar cell passivation layers are however strongly dependent on surface quality of the Si substrate as well as on the processing conditions, and the results are thus generally not directly transferable between different processing systems. Accurate characterization methods allowing for a fundamental understanding of the recombination processes for the specific passivation layer in question is therefore of high importance.

The surface recombination velocity (SRV) at a Si surface can be reduced by lowering the interface defect density (chemical passivation) or by reducing the concentration of one type of charge carriers in the region near the surface with a built-in electric field (field-effect passivation)[2]. In solar cells, such a surface band bending is normally achieved by incorporating dielectric passivation layers with fixed charges, such as a-Si:N_x:H (positive charges) or a-AlO$_x$ (negative charges). The surface potential, and thus the SRV, may also be modulated directly by applying voltage to a gate electrode placed on top of a dielectric passivation layer[3,4] or by deposition of charged ions on the surface in a corona discharge chamber[5,6]. The corona charge method has the advantage of being non-invasive (the charges can be washed off by a polar solvent), and has traditionally been the method of choice for characterization of dielectric passivation layers in solar cells. Also, gate electrodes on the sample surface will typically obstruct either the optical excitation or the photoconductance measurement that are needed in most techniques used for minority carrier lifetime measurements, like quasi-steady state photoconductance (QSSPC).

Recently we proposed a new technique for analyzing the surface recombination for passivated silicon substrates[7]. The technique is based on measurements of the effective carrier lifetime in a photoluminescence (PL) imaging setup[8] while a voltage is applied over the rear side passivation layer. In contrast to corona charging techniques, photoluminescence (PL) imaging under applied bias, hereafter referred to as PL-V, requires metal electrodes to be produced on the sample surface. However, the PL-V method allows for very fast measurements and simultaneous data collection from multiple areas on the sample. The technique also has the advantage of allowing for repeated measurement scans between inversion and accumulation, which can be recorded with little or no influence of the measurement history of the sample. In this paper we compare the results obtained by the PL-V method with quasi-steady state microwave detected photoconductance decay (QSS-μPCD) measurements performed after controlled deposition of corona charges on the surface[9]. Various aspects of the two measurement techniques and important uncertainties in the determination of the effective SRV are discussed. Finally, the measured data is compared to both an extended Shockley-Read Hall (SRH) recombination model and complementary measurements of the oxide charge density.

II. EXPERIMENTAL DETAILS

A. Sample preparation

Double-side polished float-zone (FZ) Si(100) wafers with a high bulk lifetime (> 3 ms) were used for the experiments. Samples were made from both p-type and n-type wafers with measured doping concentrations of $N_A = 5.4 \times 10^{15}$ cm^{-3} and $N_D = 1.7 \times 10^{15}$ cm^{-3} respectively. After carrying out a standard RCA (1+2) clean[10] and 30 s immersion in a 5% HF solution, the wafers were loaded into a tube furnace and oxidized in dry O$_2$ at 1000 °C for 60 min. The oxide thickness was measured by variable-angle spectroscopic ellipsometry and found to be 70-72 nm uniformly across the wafers. In order to get a comparable passivation quality for the two samples the p-type wafer received a post-oxidation forming gas (5% H$_2$, 95% N$_2$) anneal at 400 °C for 30 min. The thermal SiO$_2$ layers on these samples provide a stable, high quality surface passivation with good dielectric properties and are thus well suited for reviewing the PL-V method and comparing the results with those from other characterization methods.

For the measurements in this paper, two different types of electrodes were deposited onto the oxide layer by thermal evaporation of Al through a shadow mask: 7 mm × 7 mm electrodes were fabricated for the lifetime vs. voltage (PL-V) measurements and 0.45-2.25 mm diameter circular electrodes were fabricated for the capacitance - voltage (C-V) measurements. Finally, a low resistivity contact was made to the Si substrate by grinding down the oxide with P200 sand paper and depositing Ag in the region opposite to the electrodes used for C-V measurements.

B. The PL-V method

A schematic overview of the experimental setup for the PL-V method is shown in Figure 1 (a). Steady state carrier lifetime measurements were carried out with a LIS-R1 PL imaging setup from BT imaging with an excitation wavelength of 808 nm and a constant illumination intensity of 17.5 mW/cm^2. The PL intensity was calibrated to the effective lifetime using a quasi-steady state photoconductance (QSSPC) measurement[11] of a reference region without metal electrodes. An external voltage source was connected to the sample in order to obtain lifetime images with an applied bias over the rear side passivation layer. The excess carrier concentration Δn was then calculated from the PL intensity averaged over the electrode area as described in Ref. 7. The steady state effective lifetime can then be calculated as

$$\tau_{eff} = \frac{\Delta n}{G},$$

(1)

where G is the generation rate per volume. Before calculating the effective lifetime, the PL intensity in the region over the rear side electrodes was divided by a sample-specific correction factor of 1.36 in order to correct for the

3

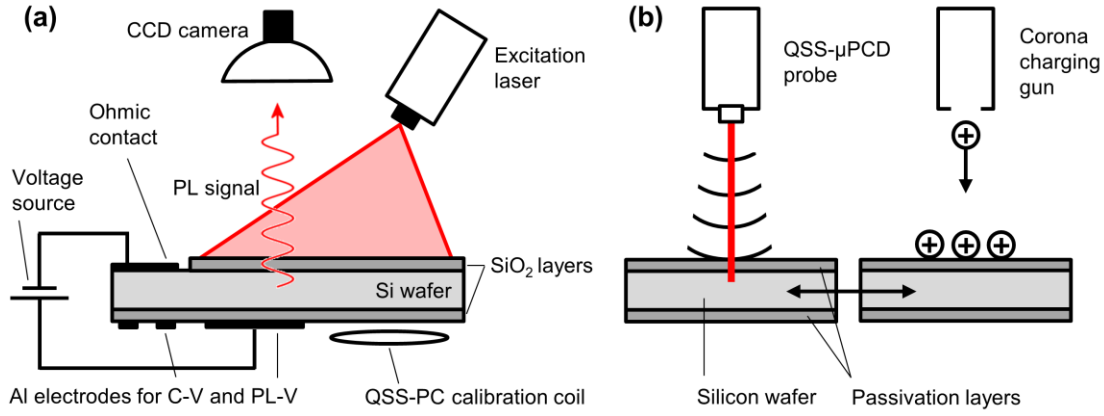enhancement of the signal caused by the higher rear side reflectivity (see section IV.A for details).

FIG. 1. Schematic overview of the experimental setup for (a) the PL-V method and (b) QSS-µPCD measurements after controlled deposition of corona charges.

C. QSS-µPCD after corona charging

With the PV-2000 multifunctional metrology platform[9], corona charge of both polarities was sequentially deposited on top of the dielectric, and the injection level dependent carrier lifetime was measured in-between as shown in Figure 1 (b). Surface voltage measurements with a vibrating Kelvin probe were incorporated after each charging step as a means to correct for the dielectric leakage current that neutralizes corona charge. The QSS-µPCD measurement combines scanning of near steady-state generation and pulsed laser excited microwave reflectance PCD monitoring. Corona charging along with the contactless measurement of the contact potential difference (CPD) in the dark and under illumination, allows measuring the flat band voltage, the corona charge needed to move the surface barrier from the initial to the flat band voltage, the interface trap density distribution in the energy gap and the net interface trapped charge. The capacitance was determined from the voltage change across the dielectric passivation layer caused by the applied corona charge.

The lifetime measured with the QSS-µPCD technique is a differential lifetime, and must therefore be integrated before it can be directly compared to the lifetime measured by QSSPC. The steady state lifetime τ_{ss} at the excess carrier concentration (injection level) Δn_{ss} can be calculated from the differential lifetime τ_{diff} as[12]

$$\tau_{ss} = \Delta n_{ss} \left(\int_0^{\Delta n_{ss}} \tau_{diff}^{-1}(\Delta n) \, d\Delta n \right)^{-1}. \tag{2}$$

III. MEASUREMENT RESULTS

The SRV of a passivated Si surface is normally calculated from measurements of the effective lifetime, which contains contributions from recombination in the bulk of the wafer and at the two surfaces. In this section we present and compare lifetime data obtained by the two measurement methods described above. The effective lifetime was measured both as a function of injection level (QSSPC and QSS-μPCD) and as a function of surface potential at a constant generation rate (PL-V and QSS-μPCD measurements after corona charging).

A. Lifetime vs. injection level

The measured differential and steady state lifetime for the p-type and n-type samples are shown as a function of injection level in Figure 2, along with the QSSPC curves used to calibrate the PL-V measurements. The photoconductance decay measurements agree well with the QSSPC curves for injection levels between approximately 3×10^{14} and 2×10^{15} cm^{-3}. The deviation at high injection levels is caused by lateral carrier diffusion causing a non-uniform carrier profile in the μPCD small spot measurement, whereas the deviation at low intensities is due to a violation of the small perturbation condition underlying the QSS-μPCD method[13]. For the PL-V and QSS-μPCD measurements a constant generation rate of $G = 2.0 \times 10^{18}$ cm^{-3}s^{-1} was therefore chosen, resulting in injection levels in the validity range of the QSS-μPCD setup.
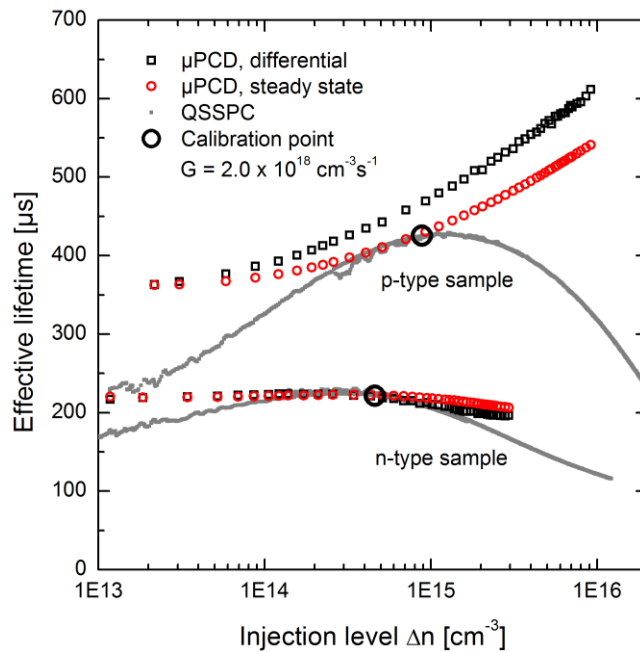

FIG. 2. *Effective lifetime as a function of injection level for the n- and p-type sample. QSSPC data (closed symbols) is shown together with QSS-μPCD data (open symbols). The injection level/lifetime point used for calibration of the PL-V data (black circle) corresponds to a generation rate of $G = 2.0 \cdot 10^{18}$ cm^{-3}s^{-1}.*

B. Lifetime vs. surface band bending

In order to compare the lifetime data obtained by the two methods, the corona charge values were converted to equivalent voltages, resulting in the same surface potential. This can be achieved by a simple charge balance: The sum of the oxide built-in charges Q_{ox} and the applied corona charge Q_{cor} must be imaged in the space charge region of the semiconductor as a charge Q_{sc} in order to fulfill the charge neutrality

$$Q_{ox} + Q_{cor} = -Q_{sc}. \tag{3}$$

If a gate electrode is used, Q_{cor} can be replaced with the induced charge in the gate electrode Q_g. Assuming that the oxide charges are located at the Si/SiO$_2$ interface, Q_g can be expressed as a function of the gate voltage V_g as[3]

$$Q_g = \frac{C_{ox}}{q}(V_g - \psi_s - \phi_{ms}), \tag{4}$$

where C_{ox} is the oxide capacitance, q is the elementary charge, ϕ_{ms} is the metal-semiconductor work function difference and ψ_s is the surface potential (amount of band bending). Using a work function for Al of 4.1 eV, ϕ_{ms} was calculated to be -0.84 eV and -0.20 eV for the p-type and n-type sample, respectively. The set of equations given by Eqs. (3) and (4) was then solved by setting $Q_{cor} = Q_g$ and inserting experimental values for the oxide charge density Q_{ox} obtained by CPD measurements in combination with corona charging. To account for ψ_s in Eq. (4) we have used the relation between Q_{sc} and ψ_s described in Ref. 4 (note that the numerical values for ψ_s are below ± 0.25 V, resulting in only a small correction). Experimental values for C_{ox} of 4.2 nF/cm^2 measured by the corona/CPD method were used in the calculations. If C_{ox} values obtained from C-V measurements (4.6-4.8 nF/cm^2) are used instead, only a slight narrowing of the QSS-µPCD versus corona curve can be observed in the final result.
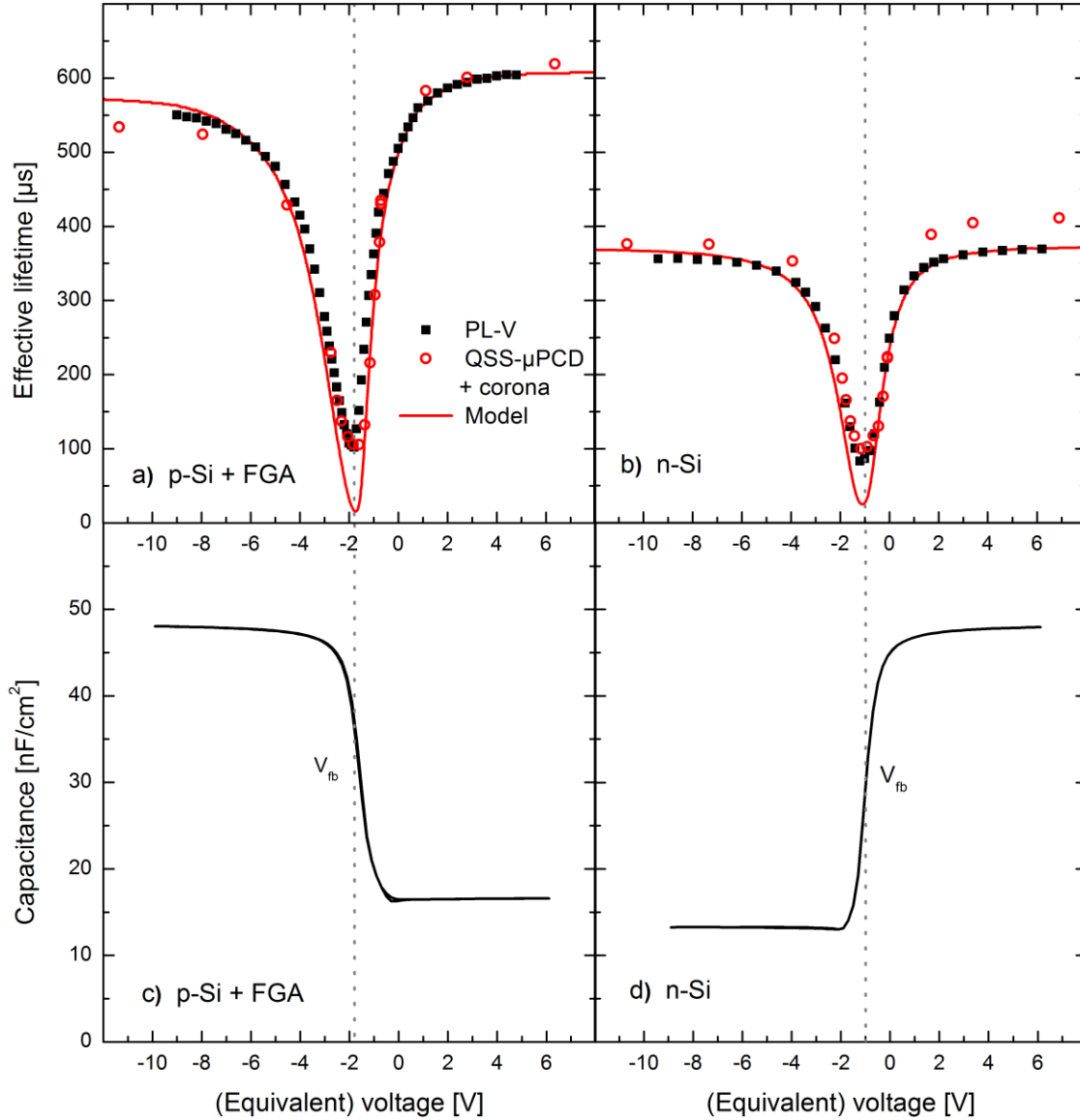
FIG. 3. Top: Effective lifetime as a function of (equivalent) voltage measured with the PL-V method and QSS-µPCD after corona charging at a constant generation rate of $G = 2.0 \times 10^{18}\ cm^{-3}s^{-1}$ for a (a) p-type and (b) n-type sample. The red solid lines show simulation results of the model described in section V. Bottom: Typical capacitance-voltage curves for a (c) p-type and (d) n-type sample. The average flat band voltage calculated from the C-V measurements is indicated by dotted vertical lines.

Figure 3 shows the effective lifetime as a function of voltage for both the p-type and n-type sample measured with the two techniques. The voltage was either directly applied in the PL-V method or calculated from the corona charge density as described above. Both samples show the same general behavior: When a small negative voltage (or charge) is applied the effective lifetime decreases as the external bias compensates the effect of the positive oxide

charge density. For increasing negative voltages, the lifetime passes through a minimum corresponding to depletion conditions at the surface, before it increases as the surface is driven into accumulation (p-type sample) or inversion (n-type sample). There is a good correspondence between the two measurement methods for both samples, with the main difference being ~15% higher absolute lifetime values measured with the corona charging method on the n-type sample. This difference is within the experimental error of the calibration of the PL-V curves, caused by inhomogeneous lifetime values across the sample. Moreover, a small shift of ~0.2 V in the position of the minimum is observed for the p-type sample.

The minimum lifetime in the PL-V curve is found to be 102 μs for the p-type sample and 83 μs for the n-type sample. For the n-type sample the lifetime vs. voltage curves are symmetrical and the curves saturates at a similar level on each side of the lifetime minimum. This indicates a similar capture cross section for electrons σ_n and holes σ_p at the interface traps. For the p-type sample the curves are slightly asymmetrical, showing highest carrier lifetime for inversion conditions at the surface, indicating that $\sigma_n > \sigma_p$, in agreement with previous findings in the literature[6].

C. Oxide charge

At flat band conditions, there is no band bending in the semiconductor, i.e. $Q_{sc} = 0$. Since Q_{sc} is monitored during the CPD measurements, Q_{ox} can easily be determined from the applied charge density that causes flat band conditions $Q_{ox} = -Q_{cor,fb}$[14].

If a gate electrode is used, Q_{ox} can be found from the induced electrode charge at the flat band voltage V_{fb}

$$Q_{ox} = -Q_{g,fb} = C_{ox}(\phi_{ms} - V_{fb})/q , \qquad (5)$$

where V_{fb} can be calculated from a high frequency C-V measurement[15]. Typical C-V curves used for these calculations and the average values for V_{fb} calculated from 10-12 measurements are shown in Figure 3. The upper part of Table I shows the oxide charge density calculated both by the corona/CPD method and from C-V curves, showing that similar values are obtained by the two techniques. The measured Q_{ox} values are found to be between 2.4 and 2.9×10^{11} cm^{-2} for both samples. Typical Q_{ox} values in the literature are in the range between 1 and 5×10^{11} cm^{-2} [16]. Note that these Q_{ox} values are in good agreement with the deposited charge density corresponding to the minimum effective lifetime, and that the measured V_{fb} corresponds well with the minimum in the PL-V curve. This behavior is expected since the surface recombination velocity is highest when the surface concentrations of electrons and holes are comparable (depending on the capture cross sections of the surface defects). This condition is met for depletion conditions at the surface i.e. in a voltage range close to V_{fb}.

IV. DISCUSSION – DETERMINATION OF THE REAR SRV

In order to obtain a fundamental physical understanding of the recombination process and compare the experimental results with a theoretical model, a precise relation must be found between the measured PL signal and the effective SRV at the rear surface. In this section we discuss various possible errors that can arise during these calculations and their impact on the final result. The four most important issues that complicate the determination of the rear side SRV in a PL-V measurement are shown schematically in Figure 4: Optical reflection from the rear electrodes, competing recombination processes in the bulk and at the front surface, lateral diffusion of charge carriers, and leakage current through the passivation layer. The latter three of these complications are also relevant for corona charging techniques. However, the combination of imaging capability and direct measurement of the voltage and current for the PL-V method simplifies the quantification of these errors.
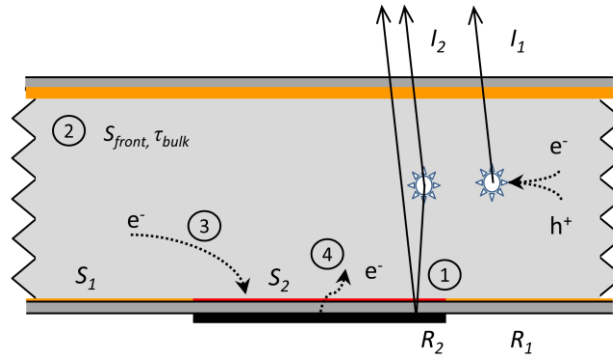
FIG. 4 Schematic overview of various effects that should be taken into account when calculating the effective SRV of the area affected by the gate electrode: 1) Signal enhancement from the increased optical reflectance of the rear side metallized regions, 2) bulk and front surface recombination contributions to the effective lifetime, 3) lateral transport of charge carriers between high and low lifetime regions and 4) leakage current through the passivation layer.

A. Effect of increased rear reflectance

The presence of metal electrodes at the rear surface locally increases the rear side reflectance in the measurement region. This causes an enhancement of the PL signal compared to the reference region, which will result in an overestimation of the carrier lifetime if this effect is not accounted for. For the PL-V measurements presented above, this effect was taken into account by experimentally measuring the enhancement of the PL intensity after placing the sample over an Al mirror made by thermal evaporation of 100 nm Al on a glass substrate. In this section we present a more fundamental and predictive description of the reflection and reabsorption in a typical PL measurement by

analytical calculations.

The spectral rate of band-to-band photon emission dB in an energy interval dE can be calculated from the intrinsic absorption coefficient α of Si as[17]

$$dB = C \, exp\left(\frac{-\eta}{k_B T}\right) E^2 \alpha(E) \, exp\left(\frac{-E}{k_B T}\right) dE \qquad (6)$$

where η is separation of the quasi-fermi energies (assumed constant in the simulations), k_B is the Boltzmann constant, T is the temperature and C contains several physical constants. The Si absorption coefficient data was taken from Ref. 19. The PL photons are emitted isotropically in all directions, but for co-planar polished samples like the ones used in this work only a very narrow range of angles will be able to escape the sample and reach the detector. The problem can therefore be treated in one dimension with negligible error. As described in Ref. 20, the vertical photon flux escaping the front surface is given by

$$\Phi_{ph}(\lambda) = \frac{B_\perp (1-R_f)}{\alpha} \frac{(1-e^{-\alpha W})(1+R_b e^{-\alpha W})}{1-R_f R_b e^{-2\alpha W}} \qquad (7)$$

where W is the sample thickness, $B_\perp$ is the emitted photon flux in the vertical direction and R_f and R_b is front and rear side reflectance, respectively. Eq. 7 is derived by integrating over the luminescence of an assumed uniform carrier distribution throughout the wafer, taking both multiple internal reflections and reabsorption into account.

Figure 5 shows both the emitted (intrinsic) photon flux and the flux that reaches the detector after being subject to reabsorption and reflection at the sample surfaces. Two different reflectance values representative for the oxidized surface and an oxidized surface with evaporated Al has been used. As seen in the figure, the total integrated signal detected by the camera is increased by 40 %, independently of the effective lifetime of the sample. This finding corresponds well with the experimentally determined signal enhancement described above, which was measured to be 36% for the oxidized samples. The deviation may be explained by small errors in the assumed reflectivity values or in the camera sensitivity function (a typical Si CCD sensitivity was used for the calculations).

The PL signal enhancement from locally increased rear reflectance can be avoided experimentally by applying a suitable short pass filter, since the highest energy photons have a large probability for reabsorption and are less likely to escape the sample after being reflected at the rear surface[20]. By placing a 1000 nm short pass filter (transmittance spectrum shown in Figure 5) in front of the camera in the PL imaging setup, the signal enhancement was reduced to ~7 % for the samples used in this paper. This number can be further reduced by using filters with a lower wavelength cut-
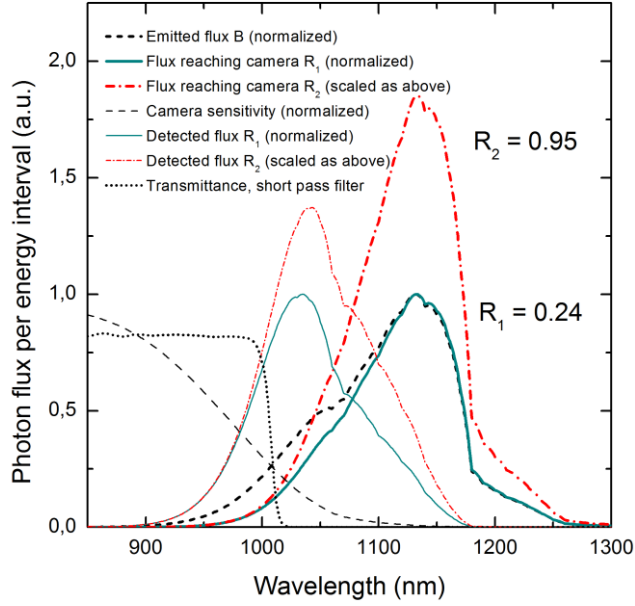
off, at the cost of reduced signal strength.

FIG. 5. P*hoton flux per energy interval as a function of wavelength, illustrating the effect of rear reflectance on the detected PL intensity. The black curve shows the theoretical band to band luminescence peak (Eq. 6) while the solid red and cyan curves show the photon flux reaching the camera after being subject to reabsorption and reflection at the sample surfaces, for two different values of the rear reflectance (Eq. 7). The dashed lines show the detected photon flux calculated from the camera sensitivity function. By applying a short pass filter, the effect of rear reflectance on the detected PL signal can be reduced.*

B. Bulk and front surface recombination

The effective lifetime is related to the front and rear SRVs S_f and S_r and the bulk lifetime τ_{bulk} by the following set of equations [21]

$$\tau_{eff} = \left(\frac{1}{\tau_{bulk}} + \alpha_0^2 D\right)^{-1} \tag{8}$$

$$tan(\alpha_0 W) = \frac{S_r + S_f}{\alpha_0 D - \frac{S_r S_f}{\alpha_0 D}}. \tag{9}$$

where D is the minority carrier diffusivity and α_0 is the smallest eigenvalue solution of Eq. 9. In order to calculate the

rear side SRV from the measured lifetime data, Eqs. 8 and 9 were solved for S_r for each measured value of τ_{eff}. High quality FZ wafers with a high bulk lifetime were used to ensure that the contribution from bulk recombination is small. Still, there is a possibility for contamination of the bulk by in-diffusion of impurities during the high temperature oxidation step, degrading the bulk lifetime of the wafers. In order to determine the bulk lifetime of the FZ wafers after oxidation a quarter of each wafer was dipped in a 5% HF solution for 1 min, cleaned by a standard RCA 1+2 clean and passivated on both sides with a 40 nm thick PECVD a-Si:H layer. This passivation ensures a SRV less than 5 cm/s, which implies that the measured effective lifetime of these samples gives a good indication of the bulk lifetime. Based on these measurements a constant bulk lifetime of 5 ms was chosen for both the n-type and p-type sample in the calculations. The errors in the rear side SRV was calculated using a minimum bulk lifetime of $\tau_{bulk} = 2.1$ ms and maximum bulk lifetime limited entirely by intrinsic recombination [22].

By using symmetrically passivated wafers the front side SRV S_f can be calculated from Eqs. 8 and 9 using the effective lifetime in a reference region which is not influenced by the metal electrodes. Another alternative, which was used in Ref. 7, is to use a known passivation layer with a low SRV on the front of the wafer, so that τ_{eff} is dominated by recombination on the rear side. We estimate the uncertainty in the determination of S_f to be 10%.

C. Effect of lateral charge carrier transport

In a PL imaging measurement, the intensity at each point is determined both by recombination in that region and diffusion of charge carriers into and out of regions that are a few diffusion lengths away. In a lifetime measurement performed by calibrated PL imaging, this can be observed as a blurring of the image on samples with high lifetimes. For the PL-V measurements this blurring effect can be clearly observed at the edges of the region affected by the external voltage, as carriers diffuse into or out of the region when the effective lifetime is lower or higher than the surrounding areas, respectively. In order to obtain a correct lifetime value the metal electrode should ideally be sufficiently large so that the measured carrier concentration (and thus the effective carrier lifetime) over the central part of the electrode is unaffected by the lateral diffusion process at the edges. The electrodes can, however, normally not be made arbitrarily large, as the probability of leakage current through pinholes or other non-uniformities in the film increases with the electrode area. Another advantage of a small electrode area is that multiple PL-V curves can be (simultaneously) measured on the same sample, allowing for improved measurement statistics and/or investigation of lateral variations in the surface properties.

In order to quantitatively investigate the magnitude of the error arising from lateral carrier diffusion during the

PL-V measurement, we have simulated the carrier density profile in a cross section of the wafer with two different fixed values for the effective SRV on the rear side, using the same geometry as shown in Figure 5. The simulation model of the sample was simplified to two dimensions by assuming a stripe electrode instead of the square electrodes that was used for the experiments. The generation rate G was calculated assuming a constant flux of 7.12×10^{16} cm^{-3}s^{-1} uniformly distributed in x-direction and a photon wavelength of 808 nm. The spatial carrier density profiles were then simulated from the 2D continuity equation, describing a plane (x,z) normal to the direction of the stripe electrode

$$G(x,z) + D\nabla^2 \Delta n(x,z) - \frac{\Delta n(x,z)}{\tau_{bulk}} = 0. \tag{10}$$

Surface recombination was accounted for by defining boundary conditions around the simulated region given by

$$\frac{d\Delta n}{dz} = -\frac{S}{D} \quad \text{(top and bottom)},$$

$$\frac{d\Delta n}{dx} = 0 \quad \text{(sides).} \tag{11}$$

Two different SRV values named S_1 and S_2 were used on the rear side as illustrated in Figure 4. The front side SRV was set equal to the rear SRV of the reference region S_1. The differential equation and boundary conditions described by Eq. 10 and Eq. 11 were solved numerically using the partial differential equation solver FlexPDE 6 [23]. An example of the simulated excess carrier density profile for a p-type wafer is shown in Figure 6.
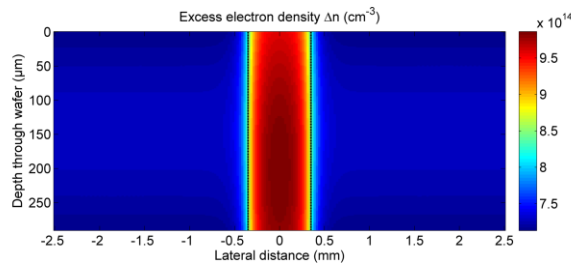

FIG. 6. Calculated excess electron density as a function of lateral distance x and depth z. The simulation was performed for a p-type Si wafer with $S_1 = 35$ cm/s and $S_2 = 15$ cm/s. The edges of the gate electrode are marked with black lines. Note the difference in scaling in the x- and z-directions.

Figure 7 shows the simulated effective lifetime as a function of lateral distance (calculated from the average Δn in the z-direction) for three different gate voltages, along with corresponding linescans taken from the calibrated PL images of the n-type sample. The experimental lifetime data is not corrected for the optical effects described above. Instead, the simulated curves are multiplied with an optical enhancement factor of 1.36 in the region over the rear electrode to account for the optical effects of the electrode in the measurement. The simulated curves correspond well with the experimental curves. The main difference is a slightly broader diffusion profile for the experimental curve as compared to that for the simulated curve. This may be caused by the fact that the simulation only takes diffusion in one dimension into account, whereas the experimental curves are affected by diffusion of carriers in both the x- and y-direction.
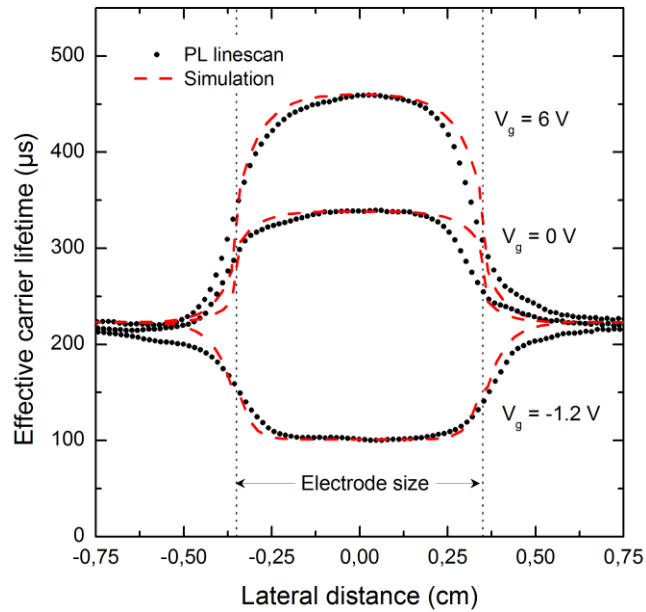

FIG. 7. *Effective carrier lifetime as a function of lateral distance over a PL-V electrode* for three different gate voltages. *Linescans from PL images (black symbols) are shown along with simulated curves (dashed lines) obtained by solving Eqs. 10 and 11, with $S_1 = 67.0$ cm/s and $S_2 = 8.8$, 37.2 and 373.6 cm/s for the top, middle and bottom curve, respectively.*

The simulated curves can be used to investigate general aspects of the effect of lateral diffusion on the measurements and the possible errors that arise for insufficient electrode sizes. One example of such an analysis is given in Figure 8, which shows the apparent (non-corrected) SRV for a p-type sample, calculated from the effective lifetime in the measurement region, as a function of the actual SRV in this region, for different electrode sizes. For an electrode width larger than 7 mm the deviation in the SRV is less than 20 % for actual SRVs in the range between ~ 8

cm/s and ~ 6000 cm/s, and the main deviation can be seen at low SRVs. This is consistent with the linescans shown in Figure 7, which shows that the scan profile in the center of the electrode region is flatter (indicating less influence of diffusion) for high SRVs compared to that observed for low SRVs.
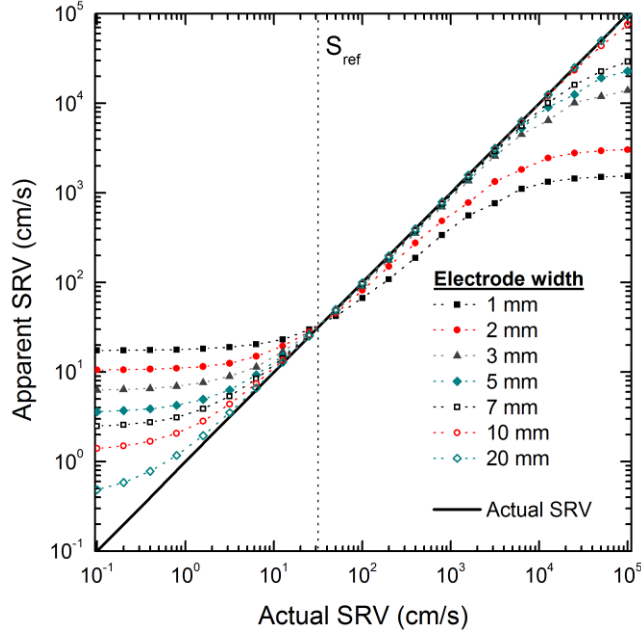

FIG. 8. Simulated apparent SRV for a p-type sample as calculated from the effective lifetime in the center of the measurement region as a function of the actual SRV in this region for different electrode sizes. The dashed line indicates the SRV of the surrounding area S_{ref}. These curves are used to estimate the error in the measured SRV arising from lateral diffusion of charge carriers into and out of the measurement region.

D. Leakage current through the oxide layer

Both when using gate electrodes and surface corona charges it is important to avoid significant leakage current through the passivation layer. For corona charges leakage currents directly affects the charge stability. A Kelvin probe can be used to measure the actual surface charge before measurements, but a significant leakage current will result in uncertainties in the charge quantification. When using a gate electrode a leakage current will not affect the stability of the surface potential, but may still influence the measurements. Charge injection into the Si wafer may result in an overestimation of the measured effective lifetime, but this effect is normally insignificant and may be neglected except in the case for large leakage currents (several mA) and very low injection conditions. A more significant effect might be a lowering of the surface potential during measurements, resulting in an overestimation of the SRV. No significant leakage current (< 1 μA) was measured during the PL-V measurements presented in this paper.

V.   SIMULATION OF THE EFFECTIVE SRV VS. VOLTAGE

A.   The extended SRH recombination model

Measurements of effective lifetime (and thus the SRV) with varying surface potential allow for a fundamental understanding of the surface recombination mechanisms, and are particularly useful for separating the contributions from field-effect and chemical passivation. In order to quantitatively extract fundamental properties of the interface traps responsible for carrier recombination we have fitted the results to an extended Shockley-Read Hall (SRH) recombination model[24]. The effective SRV at the SiO_2/c-Si interface is then calculated by integrating the SRH defect recombination over the energy-dependent continuum of interface states $D_{it}(E)$[25,26]. The SRV is strongly dependent on the surface concentration of electrons and holes n_s and p_s, which are determined by the doping concentration, the injection level and the surface potential ψ_s. In order to simulate the effective SRV as a function of applied gate voltage we have used the Girisch formalism[3,24] to determine a self-consistent value of ψ_s for any given combination of ϕ_{ms}, Q_{ox} and V_g. This is the same approach which was used to compare the effect of deposited corona charge and applied gate voltage in section III-B. To simplify the analysis we have assumed that Q_{ox} is constant with all the charges located at the SiO_2/c-Si interface and that the contribution from the charges in the interface traps Q_{it} can be neglected in the charge balance.

For the simulations we assumed a constant distribution of interface states and constant capture cross sections over the band gap. Experimental D_{it} values measured in the middle of the band gap by the CPD method described in Ref. 14 was used as input to the model.

B.   Additional surface recombination mechanisms

The measured effective SRV for an oxidized Si surface can generally not be enforced arbitrarily low by increasing the corona charge density or gate voltage. For a very high surface potential the SRV can be dominated by a process which is different from the standard SRH recombination at the surface defects. Glunz *et al.*[6] attributed this to a combination of spatial fluctuation of the surface potential caused by inhomogeneous corona charge distribution at the surface, recombination at defects in the space-charge region and shunt (tunnelling) currents of charge carriers through the potential barrier at the surface. For the polished wafers with deposited gate electrodes used in this work we do not expect the spatial fluctuations of the surface potential to be an issue. Furthermore, we observe a similar minimum SRV for the accumulated surface as compared to the inverted surface. This indicates that no significant recombination occurs in the space charge region, as the highest recombination rate is expected at the cross-over point where the

electron and hole concentrations are of similar magnitude, which only is the case for the inverted surface. For the simulation in this model we have therefore only considered the contribution from tunnelling shunt currents. The additional SRV contribution from this mechanism is given by[6]

$$S_{Rp} = \frac{V_{bulk}/R_p}{qc_0 \left(e^{qV_{bulk}/k_B T} - 1 \right)} \tag{12}$$

where R_p is the resistance of an effective shunt conductor in parallel with the standard recombination current, $V_{bulk} = \phi_p - \phi_n$ is the separation of the quasi-Fermi levels in the bulk and c_0 is the equilibrium minority carrier concentration. The total effective SRV was modelled as $S_{eff} = S_{SRH} + S_{Rp}$, where S_{SRH} is the SRV originating from the standard SRH surface recombination described above.

C. Simulation results

Figure 9 shows the effective front and rear SRV for the n-type sample as a function of applied voltage. The experimental data points are calculated from the PL-V curves shown in Figure 3 using Eqs. 8 and 9, and the error bars indicate the uncertainty calculated from the sum of the different possible errors discussed in section IV. A Nelder-Mead optimization algorithm available through the Matlab Optimization Toolbox[27] was used to find a best fit of the model described above to the experimental front and rear SRV data, using Q_{ox}, σ_n, σ_p and R_p as free fitting parameters. The solid red lines show the best fit curves, and the dashed and dotted lines show the contributions from the standard SRH model and the shunt current recombination, respectively. The same procedure was carried out for the p-type sample (data not shown). The corresponding calculated lifetime curves for both samples are shown as solid red lines in Figure 3. For both the n-type and p-type sample, we find a good agreement between the simulated curves and the experimental data, except in a small region close to the flat band voltage, where the SRV goes through a maximum. In this region the model overestimates the SRV with more than one order of magnitude for both samples, indicating that the extended SRH cannot be used to describe the surface recombination process correctly when the field effect passivation is completely removed.

The measured D_{it} values and the best fit simulation parameters for the two samples are shown in Table I, together with experimental values for the oxide charge density measured with both the CPD method and from C-V measurements. The Q_{ox} values which give the best fit to the experimental SRV vs. voltage curves are in good agreement with the measured values from the CPD and C-V measurements. From the best-fit values we find that the

σ_n is in the same order of magnitude as σ_p for both samples, with the capture cross section ratio σ_n/σ_p being 5.4 and 2.2 for the p-type and n-type sample, respectively.
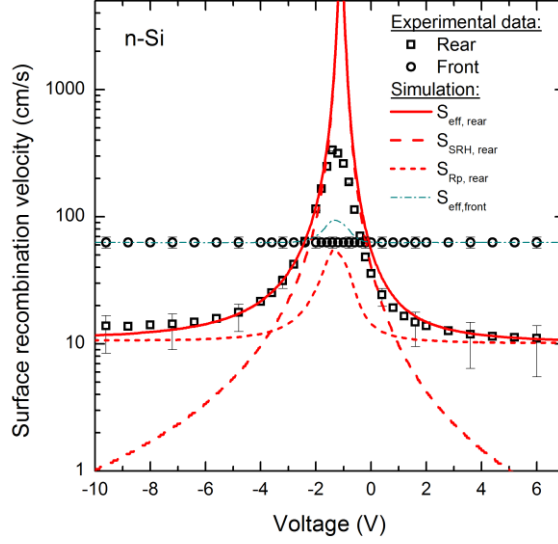

FIG. 9. *Front and rear side SRV for the n-type sample as a function of applied voltage. Experimental values calculated from the PL-V data shown in Figure 3(b) are shown together with the different simulated contributions to the effective SRV described in sections V.A and V.B. Error bars were calculated as a sum of the different uncertainties discussed in section IV.*

Experimental values

Parameter	Description	Unit	p-Si + FGA	n-Si
D_{it}	Density of interface states	cm^{-2}/eV	2.6×10^{10}	1.2×10^{11}
Q_{cor} at τ_{min}	Corona charge at τ_{min}	cm^{-2}	-2.9×10^{11}	-2.5×10^{11}
Q_{ox}	Oxide charge (from CPD)	cm^{-2}	2.7×10^{11}	2.4×10^{11}
Q_{ox}	Oxide charge (from C-V)	cm^{-2}	$(2.8 \pm 0.2) \times 10^{11}$	$(2.7 \pm 0.4) \times 10^{11}$

Fitting parameters for SRH model

Parameter	Description	Unit	p-Si + FGA	n-Si
Q_{ox}	Oxide charge	cm^{-2}	3.0×10^{11}	2.6×10^{11}
σ_n	Electron capture cross section	cm^2	1.5×10^{-14}	7.5×10^{-15}
σ_p	Hole capture cross section	cm^2	2.9×10^{-15}	3.3×10^{-15}
R_p	Equivalent shunt resistance	Ωcm^2	260	350

TABLE I. Top: Measured values for D_{it} and Q_{ox} for the two samples, together with the corona charge needed to compensate the field-effect passivation. D_{it} values are measured in the middle of the band gap by CPD measurements, whereas Q_{ox} values are determined both from CPD measurements after corona charging and C-V measurements. The numbers obtained by C-V are average values and uncertainties are calculated as two standard deviations from 10-12 measurements on different electrodes. Bottom: Fitting parameters for the extended SRH model used to calculate the curves presented in Figure 3 and Figure 9.

VI.   CONCLUSION

We have demonstrated that the recently developed PL-V method can be used to analyze the recombination activity at the SiO_2/c-Si interface under varying band bending conditions. The measured effective carrier lifetime vs. voltage curves were found to be in excellent agreement with those obtained by QSS-µPCD measurements after deposition of controlled amounts of corona charges on the sample surface. We have discussed the impact of various different error contributions with regards to determination of the rear side SRV from the measured PL intensity, and the corrections presented in this paper are a first necessary step towards a quantitative analysis of more complex sample geometries and full solar cell structures. The imaging capability and direct measurement of the potential gives an additional advantage for the PL-V method in the quantification of these errors as compared to other techniques involving local modulation of the surface potential. We have shown how the measured SRV under varying applied gate voltage can be interpreted in the framework of the extended SRH theory, in terms of the interface state density and capture cross sections of the surface defects and the fixed oxide charge density. We find a good agreement between these results and complementary measurements of the oxide charge. In addition to the standard SRH recombination an added contribution to the effective SRV, modeled as a tunneling shunt current through the surface space charge layer, was necessary to explain the experimental findings. The PL-V method allows for very fast measurements to be carried out independently of the measurement history of the sample and allows for simultaneous measurements of several areas of the wafer. Through this work we have demonstrated the method as a powerful tool for fundamental investigation of c-Si passivation layers.

REFERENCES

[1] D. Biro, S. Mack, A. Wolf, A. Lemke, U. Belledin, D. Erath, B. Holzinger, E.A. Wotke, M. Hofmann, L. Gautero, S. Nold, J. Rentsch, and R. Preu, in *Proceedings of the 34th IEEE Photovoltaic Specialists Conference*, 2009, p. 1594.

[2] A.G. Aberle, *Crystalline Silicon Solar Cells - Advanced Surface Passivation and Analysis* (Centre for Photovoltaic engineering, University of New South Wales, 1999) p. 118.

[3] R.B.M. Girisch, R.P. Mertens, and R.F. De Keersmaecker, *IEEE Trans. Electron Dev.* 35, 203 (1988).

[4] E. Yablonovitch, R.M. Swanson, W.D. Eades, and B.R. Weinberger, *Appl. Phys. Lett.* 48, 245 (1986).

[5] M. Schofthaler, R. Brendel, G. Langguth, and J.H. Werner, in *1st IEEE World Conference on Photovoltaic Energy Conversion*, Hawaii 1994, p. 1509.

[6] S.W. Glunz, D. Biro, S. Rein, and W. Warta, *J. Appl. Phys* 86, 683 (1999).

[7] H. Haug, Ø. Nordseth, E. V. Monakhov, and E.S. Marstein, *Sol. Energy Mater. Sol. Cells* 106, 60 (2012).

[8] T. Trupke, R.A. Bardos, M.C. Schubert, and W. Warta, *Appl. Phys. Lett*. 89, 44103 (2006).

[9] M. Wilson, J. D'Amico, A. Savtchouk, P. Edelman, A. Findlay, L. Jastrzebski, J. Lagowski, K. Kis-Szabo, F. Korsos, A. Toth, A. Pap, R. Kopecek, and K. Peter, in *37th IEEE Photovoltaic Specialists Conference*, Seattle, USA, 2011, pp. 1748–1753.

[10] W. Kern, *J. Electrochem. Soc.*, 137, 1887 (1990).

[11] R.A. Sinton, A. Cuevas, and M. Stuckings, *in Proceedings of the 25th IEEE Photovoltaic Specialists Conference*, Washington, D.C., USA, 1996, p. 457.

[12] J. Schmidt, *IEEE Trans. Electron Dev.* 46, 2018 (1999).

[13] M. Wilson, P. Edelman, J. Lagowski, S. Olibet, and V. Mihailetchi, *Sol. Energy Mater. Sol. Cells* 106, 66 (2012).

[14] M. Wilson, J. Lagowski, A. Savtchouk, L. Jastrzebski, and J. D'Amico, in *ASTM Conference on Gate Dielectric Oxide Integrity*, San Jose, CA, USA (1999).

[15] E. Nicollian and J.R. Brews, *MOS (metal Oxide Semiconductor) Physics and Technology* (John Wiley & Sons, Inc., 2003) p. 423.

[16] A.G. Aberle, S.W. Glunz, A.W. Stephens, and M.A. Green, *Prog. Photovoltaics* 2, 265 (1994).

[17] P. Wurfel, *J. Phys. C Solid State* 15, 3967 (1982).

[18] M.A. Green, *Sol. Energy Mater. Sol. Cells* 92, 1305 (2008).

[19] T. Trupke, M.A. Green, P. Wurfel, P.P. Altermatt, A. Wang, J. Zhao, and R. Corkish, *J. Appl. Phys* 94, 4930 (2003).

[20] J. Müller, K. Bothe, S. Herlufsen, H. Hannebauer, R. Ferré, and R. Brendel, *Sol. Energy Mater. Sol. Cells* 106, 76 (2012).

[21] A.B. Sproul, *J. Appl. Phys* 76, 2851 (1994).

[22] M.J. Kerr and A. Cuevas, *J. Appl. Phys* 91, 2473 (2002).

[23] *FlexPDE 6 User Manual*, PDE solutions Inc, www.pdesolutions.com (2011).

[24] A.G. Aberle, S. Glunz, and W. Warta, *J. Appl. Phys* 71, 4422 (1992).

[25] W. Shockley and W.T. Read Jr., *Phys. Rev.* 87, 835 (1952).

[26] D.J. Fitzgerald and a. S. Grove, *IEEE Trans. Elec. Dev.* 15, 426 (1968).

[27] *Optimization Toolbox User's Guide*, Mathworks, www.mathworks.se/help/optim/ (2009).